ACS Photonics

Article

pubs.acs.org/journal/apchd5

Band-Edge Bilayer Plasmonic Nanostructure for Surface Enhanced Raman Spectroscopy

S. Hamed Shams Mousavi, Ali A. Eftekhar, Amir H. Atabaki,[†] and Ali Adibi*

School of Electrical and Computer Engineering, Georgia Institute of Technology, Atlanta, Georgia 30332, United States

Supporting Information

ABSTRACT: Spectroscopic analysis of large biomolecules is critical in a number of applications, including medical diagnostics and label-free biosensing. Recently, it has been shown that the Raman spectroscopy of proteins can be used to diagnose several diseases, including a few types of cancer. The development of the assays based on surface enhanced Raman spectroscopy (SERS), which are suitable for large biomolecules, could lead to a substantial decrease in the amount of specimen necessary for these experiments. We present a new method to achieve high local field enhancement in SERS, through the simultaneous adjustment of the lattice plasmons and localized surface plasmon polaritons, in a periodic bilayer nanoantenna array resulting in a high enhancement factor over the sensing area, with relatively high uniformity. The proposed plasmonic nanostructure is comprised of two interacting nanoantenna layers, providing a sharp band-edge lattice plasmon mode and a wide-band localized surface plasmon for the separate enhancement of the pump and emitted Raman signals. We demonstrate the application of the proposed nanostructure for the spectral analysis of large biomolecules by binding a protein (streptavidin) selectively on the hot spots between the two stacked layers, using a low concentration solution (100 nM), and we successfully acquire its SERS spectrum.

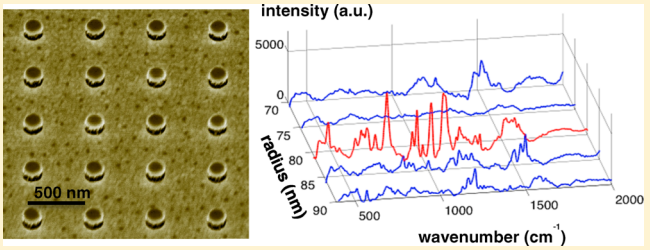

KEYWORDS: *plasmon, nanoantenna, Fano resonance, band-edge nanostructure, surface-enhanced Raman spectroscopy*

While surface-enhanced Raman spectroscopy (SERS) has been very successful for small molecules,[1−6] its application for large molecules was hampered by the complexity of the Raman signature and the nonuniformity of the SERS enhancement in most common SERS bioassays. The recent progress in the spectral assignment and Raman instrumentation has lent itself to the revival of interest in the Raman spectroscopy of proteins and other large biomolecules.[7−9] In applications such as cancer diagnosis,[10] it has been shown that valuable insights could be gained by looking into the Raman spectra of proteins, once deemed to be too complex to extract any meaningful information. Nevertheless, the vast majority of these measurements have been performed using conventional Raman spectroscopy at high concentration levels. Transformation of these experiments to SERS could be pivotal in applications, such as pathogen detection, and real-time spectral analysis in low concentration levels requiring high sensitivity, and it can lead to a substantial decrease in material cost.

A number of plasmonic structures can in essence provide the sufficient field enhancement in their hot spots for low concentration spectral analysis.[11−13] In practice, however, the reported values for the average field enhancement in these structures are fairly modest due to the large variation of the field profile over the sensing area. Moreover, in the case of large biomolecules, the nonuniformity of the enhancement profile could result in the unrepeatability of the experiments due to substantial size of the biomolecules relative to the hot-spots. The conventional route to SERS is to use the localized surface plasmon polaritons (SPP) in an array of isolated nanoantennas. The high absorption (and scattering) cross section of the localized SPPs near the resonance frequency results in a large enhancement of the Raman signal collected from the molecules located in the intense hot spots. However, there is a practical limit to the intrinsic nanoantenna cross sections, determined by the topology and material properties. A promising approach to improve the SERS enhancement is to use the sharp and asymmetric Fano-type resonances[14−22] that occur in coupled periodic plasmonic nanostructures due to the beating between the scattering caused by the periodicity of the nanostructure (i.e., Bragg effect) and the local nanoantenna scattering. These Fano-type resonant features have recently found some interesting applications. For instance, ultrasensitive refractive index sensing has been demonstrated using these resonant modes, taking advantage of their high sensitivity to any small perturbation in the environment.[23,24] More importantly, these collective resonant features are accompanied by plasmonic waves propagating across the structure, called lattice plasmons (LPs). This propagative wave is a direct consequence of the periodicity of the nanostructure, that is, Bragg effect, and is characteristically different from the surface plasmon modes in a thin metallic film, which has also been used to increase Raman enhancement in SERS.[25,26] Previously, LPs inside a nanoantenna array were used to enhance the stimulated

Received: December 30, 2014
Published: June 2, 2015

DOI: 10.1021/ph500487g
ACS Photonics 2015, 2, 1546−1551

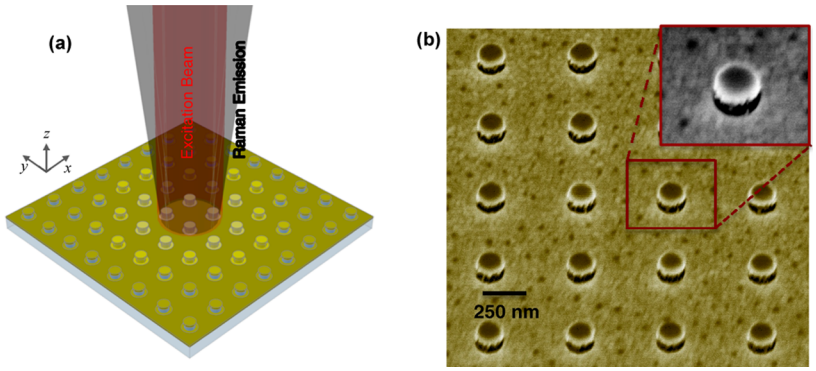

Figure 1. Band-edge bilayer plasmonic nanostructure. (a) Schematic view. (b) False-colored scanning electron microscope (SEM) image of a nanoantenna array (lattice constant of 540 nm and nanopillar radius of 80 nm in the layout) with 40° tilt angle revealing the mushroom-shaped topology of the nanoantennas with rims slightly extended after electron beam deposition.

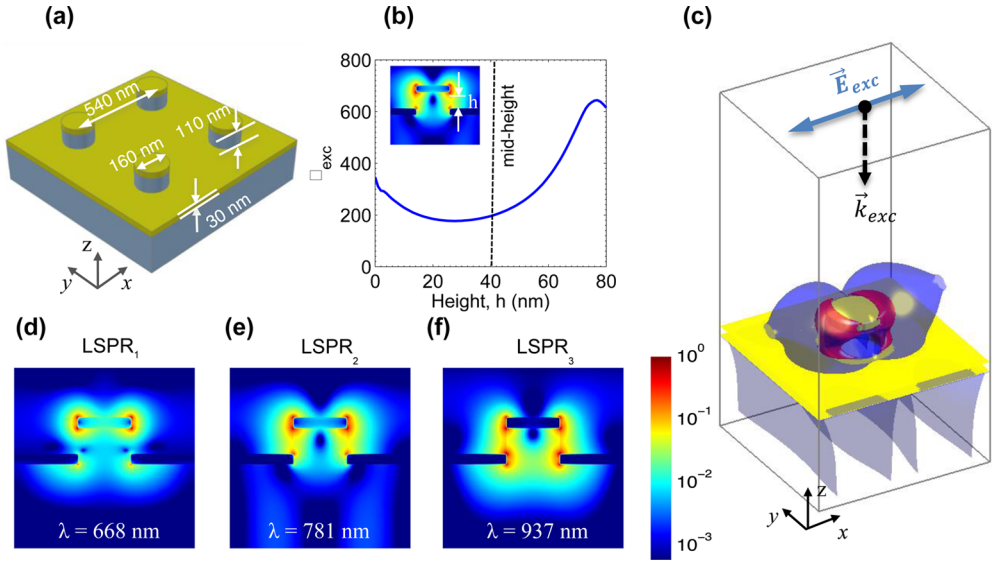

Figure 2. Distribution of the electrical field in a unit cell of the nanostructure. (a) Geometrical parameters of the periodic array. (b) Distribution of excitation field enhancement, Γ_{exc}, along the dielectric nanopillar at 5 nm radial distance, from the edge of the nanoapertures to the lower edge of the nanodisk (30 nm of the dielectric is covered by the bottom gold layer). (c) Lateral and vertical coupling inside the nanostructure; the red surface (25% of the peak Γ_{exc}) shows the lateral coupling between the two layers of the nanostructure in an individual unit-cell, whereas the blue surface (5% of the peak Γ_{exc}) portrays the slightly extended Bloch mode (LP mode) resulting in the lateral coupling between adjacent unit cells. (d–f) Normalized electric-field distribution of the three localized SPPs (x–z cross-section) at 668, 781, and 937 nm, respectively.

emission[27,28] by increasing the local density of state (LDOS) at the band-edge and, hence, the emission rate according to Fermi's golden rule.[29,30] However, this effect is very narrow-band and is not suitable for the enhancement of the wide-band Raman emission spectra.

Our approach, in this paper, is to utilize the band-edge LPs at the excitation (or pump) wavelength to increase the net absorption cross section of the array (to achieve more efficient pumping). The interaction between adjacent unit cells of the bilayer array, at the LP band-edge, slightly extends the localized SPPs in space and forms a Bloch mode with near-zero group velocity that can be coupled more efficiently with the incoming light. The SPP modes of the nanostructure are also adjusted to maximize the overall emission cross section. Furthermore, the two interacting layers of the nanostructure create intense hot spots in the vertically oriented gaps (over the dielectric nanopillars), which are coated selectively to form the sensing area. These two provisions collaboratively result in a large SERS enhancement over a large bandwidth, rivaling and potentially surpassing most nanofabricated SERS arrays. The rather uniform distribution of the SERS enhancement over the sensing area renders the structure particularly suitable for large biomolecules, such as proteins.

RESULTS AND DISCUSSION

Nanostructure Design and Theoretical Modeling. An array of gold nanodisks, stacked on an array of nanoapertures via supporting dielectric nanopillars, constitutes our nanostructure, illustrated in Figure 1a,b. The dielectric nanopillars, composed of hydrogen-silsesquioxane (HSQ), act as the sensing area in SERS measurements. In order to maximize the light–matter interaction, the periodicity of the structure is selected such that a band-edge LP with near-zero group velocity is induced at the close vicinity of the excitation wavelength, as a direct consequence of the lateral coupling between the nanoantennas. Additionally, the structure is designed to confine the localized SPP modes at the Fano resonance wavelength in the vertical gap between the two layers, providing a large and fairly uniform enhancement profile over the dielectric nanopillars (Figure 2b,c). We found that the highest enhancement

DOI: 10.1021/ph500487g
ACS Photonics 2015, 2, 1546–1551

factor occurs when the LP band-edge coincides with the resonance peak of a localized SPP resonance peak.

We performed an extensive search over the domain of the design parameters (i.e., the nanopillar radius and the lattice constant) through the full wave simulation of the structure using three-dimensional finite-difference time-domain (FDTD) method (Lumerical Inc.) to design the structure with this requirement, and the optimal design parameters are shown in Figure 2a.

The nanostructure shown in Figure 2a has three distinct localized SPP modes: a primarily disk mode at 668 nm ($LSPR_1$) and two vertical gap modes at 781 ($LSPR_2$) and 937 nm ($LSPR_3$), in which most of the energy is confined in the vertical gap between the nanoantenna and the nanoaperture (see Figure 2d–f). Both of these two gap modes provide a large field enhancement with relatively uniform distribution over the dielectric surface. Within the range of SERS measurements (wavelengths between 797 and 931 nm), the second and third resonant modes both contribute to the overall Raman enhancement. In addition, $LSPR_2$, at 781 nm, coincides with the band-edge of the second LP mode (LP_2), near the pump wavelength (785 nm), Figure 3. This Fano-type plasmonic mode is very narrow band, but it has a large absorption cross section and field enhancement at the resonance peak. Hence, $LSPR_2$ is an excellent candidate for enhancing the narrow-band pump signal, at 785 nm wavelength. The second gap mode has a considerably larger bandwidth and contributes to the enhancement of the emitted Raman signal.

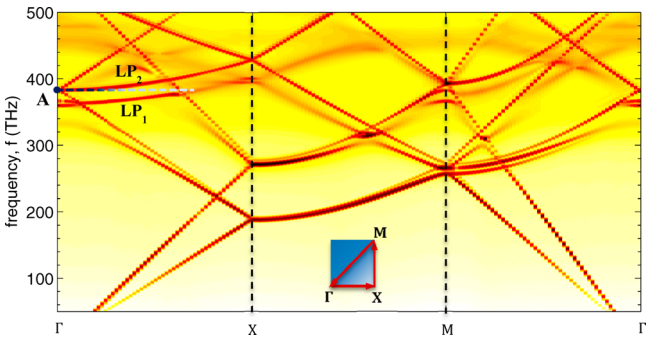

Figure 3. Full band diagram of the nanostructure shown in Figure 2a; LP_1 and LP_2 denote the LP modes, and point A shows the LP_2 band-edge, coincident with second localized SPP ($LSPR_2$) in Figure 2e, the 2D Brillouin zone used in the calculation of the band diagram is shown in the inset (this band-diagram calculation is also performed using 3D FDTD method).

The structure shown in Figure 2a has two LP modes, each one with a band-edge at normal incidence that can be adjusted in a wide frequency range by changing the lattice constant (nanopillar radius has a minor effect on the LP band-edge). On the other hand, the resonance peaks of the SPP modes of this structure can also be adjusted in a wide frequency range by changing the nanopillar radius and to some extent the lattice constant. Thus, the proposed structure can be adjusted to operate within a wide frequency gamut for the simultaneous enhancement of the excitation and emission signals. Figure 3 shows the band-diagram of the optimized nanostructure, over the 2D Brillion zone (shown in in the inset). At normal incidence ($k_x = k_y = 0$ corresponding to Γ on the horizontal axis), both LP modes have zero group velocity. In our structure, we used the second LP band-edge (point A on LP_2 band), as it can be excited more efficiently with the normally incident light and can be adjusted more easily.

To assess the performance of our structure for sensing, we have calculated the local excitation and emission field enhancement spectra, Γ_{exc} and Γ_{em}, respectively, using separate 3D FDTD simulations. Figure 4a shows the Γ_{exc} under the normal incidence (defined as the squared value of the local electric field under plane wave excitation with unit amplitude) at two fixed positions (points A and B in Figure 4a). The emission field enhancement (Γ_{em}), also known as the Purcell factor, for the three field components at point A in Figure 4a is shown in Figure 4b. In order to calculate the spontaneous emission, we have approximated the excited molecules by an electric dipole located at a fixed position point A (approximate position of the proteins attached to the nanopillars), and we have estimated the enhancement factor using the method proposed by Xu et al.[31] In contrast to most reported work in plasmonic sensing, where the target molecule is immobilized to the metallic surface, in this work the target molecules are immobilized on the dielectric surface of the nanopillars. This lowers the amount of analyte necessary for the coating of the nanostructure; an important consideration in many biosensing applications. The results shown in Figure 4a,b depict close to the worst case for (i.e., the smallest) Γ_{exc} and Γ_{em} as the point A in Figure 4a is located close to the minimal point of electric field distribution at 785 and 937 nm (Figure 2e,f). The total enhancement factor in this worst-case scenario is in the order of 10^5 at 785 nm, comparable to the maximum enhancement

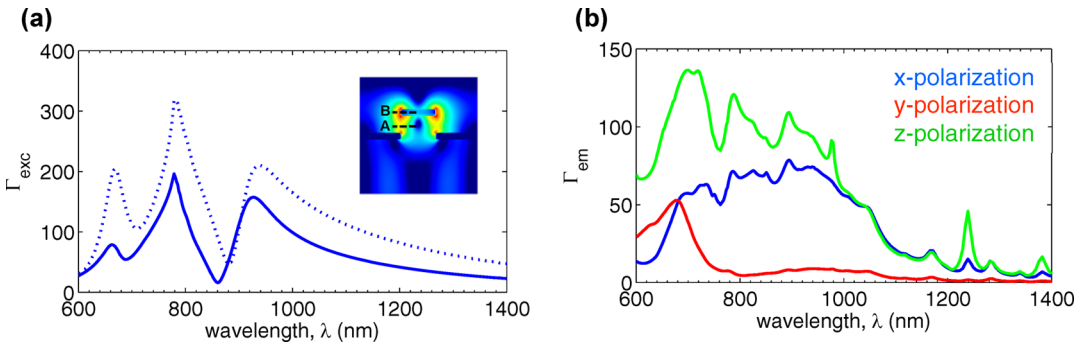

Figure 4. Excitation and emission enhancement spectra (simulation). (a) Excitation field enhancement (Γ_{exc}); the solid curve shows the enhancement profile at the midheight of the nanopillar with 5 nm radial distance (point A in the inset), and the dotted curve shows the enhancement at the midheight of the top nanodisk (point B) for the sake of comparison. (b) Enhancement factor of the spontaneous Raman emission (Γ_{em}) at point A in (a) for the *x*, *y*, and *z* components of the electric field shown by blue, red, and green curves, respectively.

DOI: 10.1021/ph500487g
ACS Photonics 2015, 2, 1546–1551

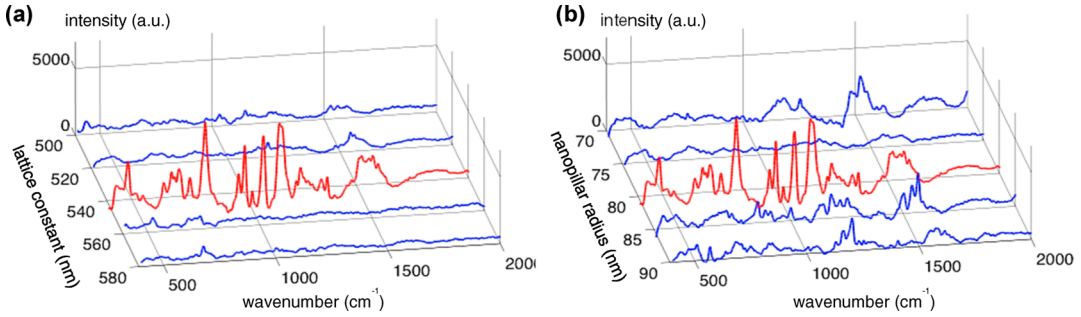

Figure 5. Comparison between the SERS spectra acquired from arrays with varying lattice constants and nanopillar radii. (a) SERS spectra acquired from the array with nanopillar radius of 80 nm and lattice constant varying between 500 and 580 nm. (b) SERS spectra acquired from the arrays with a fixed lattice constant of 540 nm and nanopillar radii varying between 70 and 90 nm; in both figures the red curve shows the SERS spectrum of the optimal array.

factor in bowtie nanoantennas, with air gaps as small as 50 nm (as one of the best fabricated nanoantennas).[32−34] The enhancement factor in our structure is higher at points that are closer to the surface of the nanopillar and are closer to the top nanodisk or the bottom nanoaperture. Most notably, the high Raman enhancement is present all over the sensing area, whereas in bowtie nanoantennas, the SERS hotspot is concentrated at a very small region between the two triangles of the nanostructure.

Surface Coating and SERS Measurements. To demonstrate the high sensitivity of our device, nanoantenna arrays with different radii and lattice constants were fabricated on a silicon wafer with a thick thermally grown SiO_2 layer on top. A medium-sized protein, streptavidin (53 kDa) was coated on the dielectric nanopillars by immersing the sample in an aquatic solution of the protein with the controlled concentration of 100 nM. Prior to the immobilization of streptavidin, the dielectric surface was functionalized using a process involving two self-assembled monolayers (SAMs), a layer of 3-aminopropyl-triethoxysilane (APTES) to provide free amine groups and a second SAM of NHS-biotin, as the linker to trap the protein molecules.

The SERS spectrum of each array was collected using a near-infrared excitation laser at 785 nm. Figure 5a shows the Raman spectra for arrays with the lattice constants varying from 500 to 580 nm and with the fixed pillar radius of 80 nm (in the layout). As expected from the simulations (see Figure 3), the best Raman signal was acquired from the array with the lattice constant of 540 nm, Figure 5a. The variation of the SERS signal with the nanopillar radius, at a fixed lattice constant is less prominent with the strongest signal acquired from the array with 80 nm radius nanopillars, Figure 5b. Our simulations had predicted that the band-edge of LP_2 should coincide with the second localized SPP resonance in the array with 80 nm nanopillars and the periodicity of 540 nm, which was confirmed with the experiments. In Figure 6, we have provided the SERS spectrum from the optimal array before and after coating the protein, as well as the Raman signature of the bulk protein (aquatic solution). In the collected SERS signal after coating, the contribution of the protein is dominant and we were able to find most of the Raman bands of bulk streptavidin in the SERS spectra. We were able to find most of the Raman bands in bulk protein in the collected SERS signal with a precision of 6 cm^{-1}.

It should be noted that fabricated nanoantennas have slightly different topology, from the ideal structure shown in Figure 2a. Close inspection by scanning electron microscopy (SEM) has revealed that the fabricated nanoantennas are mushroom-

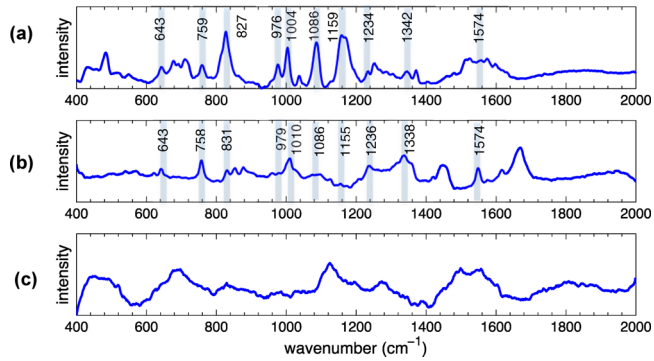

Figure 6. Band assignment in the SERS spectrum collected from the optimal array. (a) SERS spectrum acquired from streptavidin and underlying SAMs (APTES and NHS-biotin) coated on the nanopillars, (b) Raman spectrum of bulk streptavidin (aquatic solution), (c) SERS spectrum acquired only from the SAM layers (APTES and NHS-biotin).

shaped (Figure 1b) with rims slightly extended outside the supporting nanopillars due to the nature of the electron beam deposition. This should also affect the geometry of the nanoapertures at the bottom of the nanopillars. Despite this nonideal shape, a good agreement between the theoretical prediction and the experiment was observed, suggesting that performance of our nanostructure is not sensitive to the impact of the fabrication imperfections on the topology of the nanoantennas.

CONCLUSION

In summary, we have presented here a novel bilayer plasmonic substrate for chip-scale SERS-based spectroscopic analysis of large biomolecules. Through the optimization of the horizontal coupling of the nanoantennas in the array, we were able to drastically improve the Raman scattering cross section of the nanoantenna array. The vertical coupling between the two layers further increases the energy confinement in the vertical gaps and provides a more uniform enhancement profile over the dielectric nanopillars. By opting for the dielectric nanopillar as the immobilization surface, the target molecules are more efficiently excited and all contribute significantly to the overall collected Raman signal. In other words, all the target molecules are bound to the surface coating at the hot-spots. These two effects collectively result in a large improvement in the overall efficiency of the SERS-based assay.

DOI: 10.1021/ph500487g
ACS Photonics 2015, 2, 1546−1551

In experiments, we have successfully acquired the SERS spectrum of streptavidin, as an example of a large biomolecule, at the concentration of 100 nM using the optimized nanoantenna array, which to the best of our knowledge, shows a 5-fold improvement compared to the previously reported plasmonic works.[35] Although we have used radially symmetric nanoantennas in this work to keep the sensitivity of the array to polarization as low as possible, the idea of using LP modes to increase the scattering cross section can be applied to other nanoantenna geometries to achieve even higher SERS enhancements. Our fabrication process is a great advantage in this regard, since higher aspect ratios and smaller gaps can be achieved using this method as compared to fabrication processes based on the lift-off or ion-beam milling.

METHODS

Fabrication of the Nanostructure. The nanoantenna arrays were fabricated on a SiO_2 wafer (4 μm of thermally grown SiO_2 on top of a silicon wafer) to minimize the fluorescence background. The oxide wafer was first covered by 110 nm of hydrogen-silsesquioxane (HSQ), which is a negative electron-beam resist and a spin-on dielectric material. Then, the thin HSQ layer was patterned using electron-beam lithography to form the nanopillars, and 100 × 100 arrays with different nanopillar radii and lattice constants were formed on the oxide surface. Finally, 3 nm of titanium and 30 nm of gold were deposited using electron-beam deposition to form the self-aligned bilayer nanostructure using a single lithography step.

Surface Functionalization. Attachment sites for streptavidin were prepared by forming two stacked SAMs on the dielectric nanopillars. First, the sample was soaked in a 4% solution of APTES (Sigma-Aldrich) in pure ethanol at room temperature for 2 h to form frees amine groups. After washing the sample in ethanol, it was soaked again in a 1 mg/mL solution of NHS-biotin (Pierce Biotechnology) in dimethyle solfoxide (DMSO) for an additional 2 h, also at room temperature, forming a second monolayer with biotin attachment sites for trapping streptavidin. Finally, the sample was soaked in an aquatic solution of streptavidin with the controlled concentration of 100 nM at 4 °C for 1 h.

Acquisition of the SERS Spectra. The Raman spectra were acquired using a commercial Raman spectrometer (Renishaw Inc.) coupled to an inverted microscope. A 50× objective lens with the numerical aperture of 0.75 was used to focus about 1 mW power from a near-infrared laser (wavelength: 785 nm) on the sample. The Raman signal was acquired in the range of 400 to 2000 cm^{-1} with 3 min acquisition time.

ASSOCIATED CONTENT

Supporting Information

Detailed fabrication process, numerical simulation techniques, and optical characterization methods. The Supporting Information is available free of charge on the ACS Publications website at DOI: 10.1021/ph500487g.

AUTHOR INFORMATION

Corresponding Author

*E-mail: ali.adibi@ece.gatech.edu. Phone: 404.385.2738. Fax: 404.894.4641.

Present Address

[†]Research Laboratory of Electronics, Massachusetts Institute of Technology, 77 Massachusetts Ave., Cambridge, Massachusetts 02139, U.S.A. (A.H.A.).

Notes

The authors declare no competing financial interest.

ACKNOWLEDGMENTS

This work was supported Defense Advanced Research Projects Agency (DARPA) under Contract No. HR 0011−10−1−0075. The authors would like to thank F. Ghasemi for sharing his surface functionalization recipe. They also thank S. R. Panikkanvalappil, M. Mahmoud, and M. El-Sayed for providing access to their setup and helping with the Raman measurements.

ABBREVIATIONS

LP, lattice plasmon; SPP, surface plasmon polariton; SP, surface plasmon; LSPR, localized surface plasmon resonance; SERS, surface enhanced Raman spectroscopy; LDOS, local density of states; FDTD, finite-difference time-domain; SAM, self-assembled monolayer; HSQ, hydrogen-silsesquioxane; APTES, 3-aminopropyl-triethoxysilane; NHS, *N*-hydroxysuccinimide

REFERENCES

(1) Kneipp, K.; Wang, Y.; Kneipp, H.; Perelman, L. T.; Itzkan, I.; Dasari, R. R.; Feld, M. S. Single molecule detection using surface-enhanced Raman scattering (SERS). *Phys. Rev. Lett.* **1997**, *78*, 1667.

(2) Nie, S.; Emory, S. R. Probing single molecules and single nanoparticles by surface-enhanced Raman scattering. *Science* **1997**, *275*, 1102−1106.

(3) Barnes, W. L.; Dereux, A.; Ebbesen, T. W. Surface plasmon subwavelength optics. *Nature* **2003**, *424*, 824−830.

(4) Lal, S.; Link, S.; Halas, N. J. Nano-optics from sensing to waveguiding. *Nat. Photonics* **2007**, *1*, 641−648.

(5) Novotny, L.; Hulst, N. V. Antennas for light. *Nat. Photonics* **2011**, *5* (no. 2), 83−90.

(6) Schuller, J. A.; Barnard, E. S.; Cai, W.; Jun, Y. C.; White, J. S.; Brongersma, M. L. Plasmonics for extreme light concentration and manipulation. *Nat. Mater.* **2010**, *9*, 193−204.

(7) Tuma, R. Raman spectroscopy of proteins: from peptides to large assemblies. *J. Raman Spectrosc.* **2005**, *36*, 307−319.

(8) Callender, R.; Deng, H. Nonresonance Raman difference spectroscopy: a general probe of protein structure, ligand binding, enzymatic catalysis, and the structures of other biomacromolecules. *Annu. Rev. Biophys. Biomol. Struct.* **1994**, *23*, 215−245.

(9) Thomas, G. J., Jr Raman spectroscopy of protein and nucleic acid assemblies. *Annu. Rev. Biophys. Biomol. Struct.* **1999**, *28*, 1−27.

(10) Gniadecka, M.; Philipsen, P. A.; Sigurdsson, S.; Wessel, S.; Nielsen, O. F.; Christensen, D. H.; Hercogova, J.; et al. Melanoma diagnosis by Raman spectroscopy and neural networks: structure alterations in proteins and lipids in intact cancer tissue. *J. Invest. Dermatol.* **2004**, *122*, 443−449.

(11) Talley, C. E.; Jackson, J. B.; Oubre, C.; Grady, N. K.; Hollars, C. W.; Lane, S. M.; Huser, T. R.; Nordlander, P.; Halas, N. J. Surface-enhanced Raman scattering from individual Au nanoparticles and nanoparticle dimer substrates. *Nano Lett.* **2005**, *5*, 1569−1574.

(12) Jackson, J. B.; Westcott, S. L.; Hirsch, L. R.; West, J. L.; Halas, N. Controlling the surface enhanced Raman effect via the nanoshell geometry. *J. Appl. Phys. Lett.* **2003**, *82*, 257−259.

(13) Li, J. F.; Huang, Y. F.; Ding, Y.; Yang, Z. L.; Li, S. B.; Zhou, X. S.; Fan, F. R.; et al. Shell-isolated nanoparticle-enhanced Raman spectroscopy. *Nature* **2010**, *464*, 392−395.

(14) Auguié, B.; Barnes, W. L. Collective resonances in gold nanoparticle arrays. *Phys. Rev. Lett.* **2008**, *101*, 143902.

DOI: 10.1021/ph500487g
ACS Photonics 2015, 2, 1546−1551

(15) Luk'yanchuk, B.; Zheludev, N. I.; Maier, S. A.; Halas, N. J.; Nordlander, P.; Giessen, H.; Chong, C. T. The Fano resonance in plasmonic nanostructures and metamaterials. *Nat. Mater.* **2010**, *9*, 707−715.
(16) Hicks, E. M.; Zou, S.; Schatz, G. C.; Spears, K. G.; Van Duyne, R. P.; Gunnarsson, L.; Rindzevicius, T.; Kasemo, B.; Käll, M. Controlling plasmon line shapes through diffractive coupling in linear arrays of cylindrical nanoparticles fabricated by electron beam lithography. *Nano Lett.* **2005**, *5*, 1065−1070.
(17) Stuart, H. R.; Hall, D. G. Enhanced dipole-dipole interaction between elementary radiators near a surface. *Phys. Rev. Lett.* **1998**, *80*, 5663.
(18) Lamprecht, B.; Schider, G.; Lechner, R. T.; Ditlbacher, H.; Krenn, J. R.; Leitner, A.; Aussenegg, F. R. Metal nanoparticle gratings: influence of dipolar particle interaction on the plasmon resonance. *Phys. Rev. Lett.* **2000**, *84*, 4721−4724.
(19) Giannini, V.; Vecchi, G.; Gómez Rivas, J. Lighting up multipolar surface plasmon polaritons by collective resonances in arrays of nanoantennas. *Phys. Rev. Lett.* **2010**, *105*, 266801.
(20) Zhou, W.; Odom, T. W. Tunable subradiant lattice plasmons by out-of-plane dipolar interactions. *Nat. Nanotechnol.* **2011**, *6*, 423−427.
(21) Väkeväinen, A. I.; Moerland, R. J.; Rekola, H. T.; Eskelinen, A. P.; Martikainen, J. P.; Kim, D. H.; Torma, P. Plasmonic surface lattice resonances at the strong coupling regime. *Nano Lett.* **2013**, *14*, 1721−1727.
(22) Chu, Y.; Schonbrun, E.; Yang, T.; Crozier, K. B. Experimental observation of narrow surface plasmon resonances in gold nanoparticle arrays. *Appl. Phys. Lett.* **2008**, *93*, 181108.
(23) Ronen, A.; Yanik, A. A.; Amsden, J. J.; Kaplan, D. L.; Omenetto, F. G.; Hong, M. K.; Erramilli, S.; Altug, H. Ultra-sensitive vibrational spectroscopy of protein monolayers with plasmonic nanoantenna arrays. *Proc. Natl. Acad. Sci. U.S.A.* **2009**, *106*, 19227−19232.
(24) Malyarchuk, V.; Stewart, M. E.; Nuzzo, R. G.; Rogers, J. A. Spatially resolved biosensing with a molded plasmonic crystal. *Appl. Phys. Lett.* **2007**, *90*, 203113.
(25) Yizhuo, C.; Banaee, M. G.; Crozier, K. B. Double-resonance plasmon substrates for surface-enhanced Raman scattering with enhancement at excitation and stokes frequencies. *ACS Nano* **2010**, *4*, 2804−2810.
(26) Yizhuo, C.; Crozier, K. B. Experimental study of the interaction between localized and propagating surface plasmons. *Opt. Lett.* **2009**, *34*, 244−246.
(27) Zhou, W.; Dridi, M.; Suh, J. Y.; Kim, C. H.; Wasielewski, M. R.; Schatz, G. C.; Odom, T. W. Lasing action in strongly coupled plasmonic nanocavity arrays. *Nat. Nanotechnol.* **2013**, *8*, 506−511.
(28) van Beijnum, F.; van Veldhoven, P. J.; Geluk, E. J.; de Dood, M. J.A.; Gert, W.; van Exter, M. P. Surface plasmon lasing observed in metal hole arrays. *Phys. Rev. Lett.* **2013**, *110*, 206802.
(29) Novotny, L.; Hecht, B. *Principles of Nano-Optics*; Cambridge University Press: U.K., 2012.
(30) Baba, T. Slow light in photonic crystals. *Nat. Photonics* **2008**, *2*, 465−473.
(31) Xu, Y.; Lee, R. K.; Yariv, A. Quantum analysis and the classical analysis of spontaneous emission in a microcavity. *Phys. Rev. A* **2000**, *61*, 033807.
(32) Schuck, P. J.; Fromm, D. P.; Sundaramurthy, A.; Kino, G. S.; Moerner, W. E. Improving the mismatch between light and nanoscale objects with gold bowtie nanoantennas. *Phys. Rev. Lett.* **2005**, *94*, 017402.
(33) Kinkhabwala, A.; Yu, Z.; Fan, S.; Avlasevich, Y.; Müllen, K.; Moerner, W. E. Large single-molecule fluorescence enhancements produced by a bowtie nanoantenna. *Nat. Photonics* **2009**, *3*, 654−657.
(34) Fromm, D. P.; Sundaramurthy, A.; Schuck, P. J.; Kino, G.; Moerner, W. E. Gap-dependent optical coupling of single "bowtie" nanoantennas resonant in the visible. *Nano Lett.* **2004**, *4*, 957−961.
(35) Galarreta, B. C.; Norton, P. R.; Lagugné-Labarthet, F. SERS detection of streptavidin/biotin monolayer assemblies. *Langmuir* **2011**, *27*, 1494−1498.

NOTE ADDED AFTER ASAP PUBLICATION

This paper was originally published ASAP on July 21, 2015. Due to a production error, panel f of Figure 2 was omitted. The corrected version was reposted on July 23, 2015.

DOI: 10.1021/ph500487g
ACS Photonics 2015, 2, 1546−1551